Journal of Alloys and Compounds 501 (2010) 159–163

Contents lists available at ScienceDirect

Journal of Alloys and Compounds

journal homepage: www.elsevier.com/locate/jallcom

XAFS studies of ytterbium doped lead-telluride

I. Radisavljević[a,*], N. Novaković[a], N. Romčević[b], M. Manasijević[a], H.-E. Mahnke[c], N. Ivanović[a]

[a] Vinča Institute of Nuclear Sciences, University of Belgrade, P.O. Box 522, 11001 Belgrade, Serbia
[b] Institute of Physics, University of Belgrade, Pregrevica 118, 11000 Belgrade, Serbia
[c] Helmholtz-Zentrum Berlin für Materialien und Energie GmbH, D-14109 Berlin, Germany

ARTICLE INFO

Article history:
Received 3 February 2010
Received in revised form 28 March 2010
Accepted 1 April 2010
Available online 20 April 2010

Keywords:
XAFS
Lead-telluride
Yb mean valence

ABSTRACT

X-ray Absorption Fine Structure (XAFS) measurements were performed on uniformly doped PbTe:Yb (1.3 at.%) at all elemental absorption edges and the analysis of the results has provided precise information on the local structure around each atom. From the near edge part of the absorption spectra it was determined that Yb is in the mixed valent state, which is predominantly divalent with a small trivalent contribution. The analysis of the high energy region of the absorption spectra revealed that Yb incorporation causes deformation of the host PbTe lattice, manifested through extension of all the nearest-, and next-nearest neighbour distances.

1. Introduction

Lead-telluride-based semiconductors are widely used in infrared (IR) optoelectronics and thermoelectronics [1–5]. They are characterized by tunable direct energy gap, high efficiency of radiative recombination, high values of static dielectric constant, small effective mass of carriers, etc. Doping with certain impurities can help to achieve Fermi level (E_F) pinning and long-term relaxation processes, such as persistent conductivity which enables construction of extremely sensitive far IR photodetectors [1]. These effects are ascribed to formation of deep defect states in energy spectrum of semiconductor, and are common for group III impurities (In and Ga, in particular). Appearance of impurity states that stabilize E_F has been observed also in Yb doped PbTe-based alloys [6–8], although it is believed that the mechanism itself is substantially different. Ytterbium modifies electronic spectrum of PbTe in a different way than In and Ga, and its introduction leads to increase of the band gap [9]. The impurity levels of In and Ga are narrow, but that of Yb is rather broad [6]. Further, while the position of pinned E_F is independent of In and Ga concentration, it does depend on Yb concentration [7,8]. The most intriguing observation related to all impurities in question is their mixed-valence behaviour in PbTe and related alloys. It is believed that In and Ga valence change from nominal 2+ to a mixture of 1+ and 3+ states [10], and that Yb valence switches by one (i.e. from non-magnetic Yb^{2+} to magnetic Yb^{3+}). Ytterbium is typical divalent metal with ground state electronic configuration $4f^{14}5d^{0}6s^{2}$. It enters the Pb sub-lattice in PbTe by replacing Pb^{2+} ion and hence a non-magnetic Yb^{2+} state is expected. However, impurity-induced magnetic response related to the presence of magnetically active Yb^{3+} ions is observed in a number of PbTe-based alloys [7,8]. This change of the Yb valence state is ascribed to change of the *f*-shell occupancy, from 14 electrons in Yb^{2+} to 13 electrons in Yb^{3+} state ($4f^{13}5d^{1}6s^{2}$), and is accompanied with charge redistribution in the local surrounding of the impurity atom. A significant distortion of the host structure around impurities was already observed in numerous PbTe-based compounds [11,12].

The aim of this paper is to determine the local structures around all atoms in PbTe:Yb and to reveal how Yb incorporation affects the host PbTe lattice. Special attention is paid to exact determination of Yb valence and its temperature stability. To that end XAFS spectroscopy was employed, since it is a powerful technique for local structures and electronic distributions determination, which are lacking for PbTe:Yb. The analysis comprises both the near edge (XANES-X-ray Absorption Near Edge Structure) and the high energy region (EXAFS-Extended X-ray Absorption Fine Structure) of the absorption spectra. The obtained results are discussed and related to available data for PbTe:Yb system.

2. Measurements and data processing

XAFS measurements were performed on PbTe uniformly doped with 1.3 at.% Yb. Tellurium K-edge, and Pb and Yb L_{III}-edge XAFS data were collected at beamline X1 of HASYLAB (DESY). The synchrotron radiation source was operating at electron beam

* Corresponding author at: Vinča Institute of Nuclear Sciences, University of Belgrade, Lab 011, Mike Petrovica-Alasa 12-14, P.O. Box 522, 11001 Belgrade, Serbia. Tel.: +381 11 3408610; fax: +381 11 3440100.
E-mail address: iva@vinca.rs (I. Radisavljević).

0925-8388/$ – see front matter © 2010 Elsevier B.V. All rights reserved.
doi:10.1016/j.jallcom.2010.04.068

energy of 4.5 GeV with a maximum stored current of 200 mA. Samples were oriented at 45° to the incident beam, and a 7-segment Ge-detector was used to collect spectra in the fluorescence mode. Multiple scans were taken to improve signal-to-noise ratio. Data analysis was performed using ATHENA and ARTEMIS packages [13]. The self-absorption attenuation of the amplitudes of the Te K- and Pb L_{III}-edge spectra was corrected using Booth algorithm [13]. The energy dependent oscillatory part of the measured X-ray absorption coefficient $\mu(E)$ was background-corrected by a smooth spline function $\mu_0(E)$, and normalized according to the standard procedure [14]. XANES spectra were modelled with the real space multiple scattering code FEFF8.2 [15], using the self-consistent field approach with Hedin–Lundqvist exchange-correlation. ARTEMIS package [13] was used to analyze EXAFS data. Fourier transforms (FT) of the EXAFS function $\chi(k) = (\mu(k) - \mu_0(k))/\Delta\mu(k)$ (k-photoelectron wave vector) were taken over the k-range between $k_{min} = (2.0, 3.0)$ Å^{-1} and $k_{max} = (12, 14)$ Å^{-1}, using the Hanning window. The k_{min} and k_{max} values were chosen at $\chi(k)$ node points to minimize the spectral broadening. To minimize the unphysical peaks in the low region of the FT($\chi(k)$), $R_{bkg} = 1.6$ was used. In the fitting procedure following parameters were varied: the mean distance of the jth shell (R_j), the number of atoms in the jth shell (N_j), the mean-squared displacement of atoms in the jth shell (σ_j^2), and the single edge shift correction (ΔE_0). For each absorption edge, the value of amplitude reduction factor S_0^2 was estimated from $\sigma^2(S_0^2)$ dependence for $k\chi(k)$, $k^2\chi(k)$ and $k^3\chi(k)$. The stability of each particular fit was checked by changing k-weights of the $\chi(k)$ function, and by performing the fitting procedure both in k- and in R-space. The fit-quality factor R, estimated by the reduced chi-square method (χ_ν^2) [13], was less than 4% for all reported results.

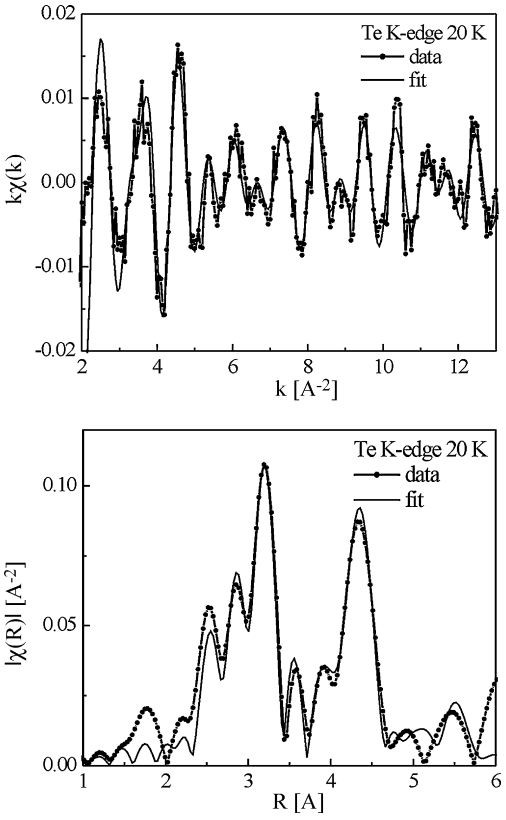

Fig. 1. Fits in k- and R-space of PbTe:Yb(1.3 at.%) EXAFS spectra taken at Te K-edge at 20 K.

3. Results and discussion

3.1. EXAFS

The fits in k- and R-space of the EXAFS spectra taken at Te K-, Pb L_{III}- and Yb: L_{III}-edge at 20 K, are presented in Figs. 1–3, respectively. The results are summarized in Table 1. From the low temperature data we were able to determine structural parameters up to the third coordination shell around all atoms (see Table 1). At RT (not presented in Figs. 1–3) the EXAFS oscillations are suppressed beyond the second coordination making the third coordination practically undetectable.

In reference to pure PbTe, the nearest-, and next- nearest neighbour distances around all atomic positions are elongated, and almost independent of temperature (see Fig. 4). The most elongated of all, Yb–Te distance is ≈3% longer than corresponding distance in YbTe (3.18 Å [16]), and ≈1.5% longer than Pb–Te distance in pure PbTe (3.23 Å [17]). The observed increase of Pb–Te distance, as obtained from Te: K- and Pb: L_{III}-edges, is approximately 1% compared to pure PbTe. The discrepancies from the PbTe-values are becoming smaller when going toward further coordinations, and already the third coordination atoms' distances approach the value 5.595 Å [17] of the average distance in PbTe (see Table 1 and Fig. 4). These results imply that the structural perturbation introduced by Yb incorporation in PbTe is of a local nature.

YbTe has the same NaCl-type structure (space group Fm3m) as the host PbTe, with slightly smaller lattice parameter ($a_{YbTe} = 6.359$ Å [16], $a_{PbTe} = 6.462$ Å [17]). It has been claimed that for Yb concentration in the range 0.5–2 at.%, the lattice constant of PbTe:Yb decreases approximately linearly with increasing Yb content [18], which is in contradiction with the bonds elongation found in this work. One should, however, bear in mind that the nature of bonding in PbTe is rather complicated and

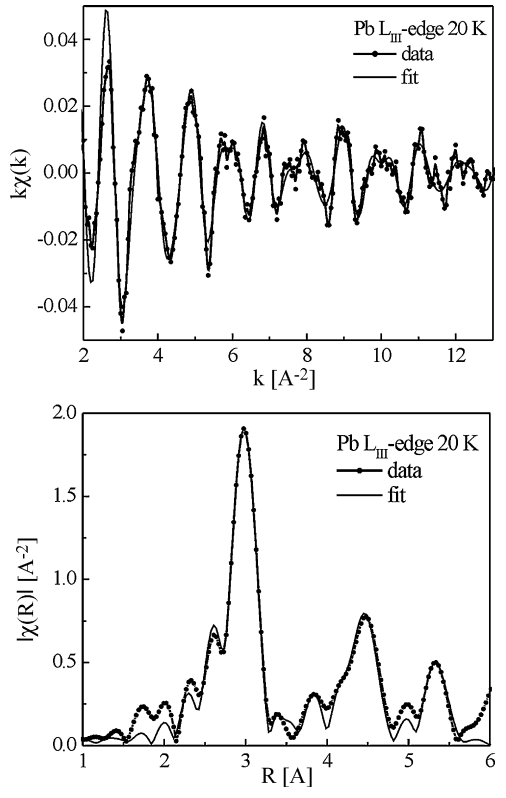

Fig. 2. Fits in k- and R-space of PbTe:Yb(1.3 at.%) EXAFS spectra taken at Pb L_{III}-edge at 20 K.

Table 1
Results of the Te K-, Pb L_{III}- and Yb L_{III}-edge EXAFS data fits of PbTe:Yb(1.3 at.%) at 20 K and RT.

	Parameter	20 K			RT	
		Coordination			Coordination	
		First Te–Pb_I	Second Te–Te	Third Te–Pb_{II}	First Te–Pb_I	Second Te–Te
Te K-edge	R [Å]	3.248(5)	4.591(7)	5.63(2)	3.30(2)	4.62(8)
	σ^2 [Å^2]	0.0013(5)	0.0022(6)	0.002(2)	0.008(2)	0.024(7)
	E_0 [eV]	7.3(6)	7.8(8)	7.3*	1.9(9)	3(2)
	S_0^2	0.53(7)			0.51(7)	
	Parameter	20 K			RT	
		Coordination			Coordination	
		First Pb–Te_I	Second Pb–Pb	Third Pb–Te_{II}	First Pb–Te	Second Pb–Pb
Pb L_{III}-edge	R [Å]	3.250(3)	4.595(7)	5.60(1)	3.28(1)	4.59(4)
	σ^2 [Å^2]	0.0034(4)	0.0041(6)	0.005(1)	0.013(2)	0.02(1)
	E_0 [eV]	0.6(3)	−1.6(5)	0.6*	1.3(6)	1.3*
	S_0^2	0.74(4)			0.71(8)	
	Parameter	20 K			RT	
		Coordination			Coordination	
		First Yb–Te_I	Second Yb–Pb	Third Yb–Te_{II}	First Yb–Te_I	Second Yb–Pb
Yb L_{III}-edge	R [Å]	3.284(5)	4.61(1)	5.60(1)	3.31(3)	4.63(6)
	σ^2 [Å^2]	0.0018(6)	0.003(1)	0.002(1)	0.010(4)	0.010(6)
	E_0 [eV]	4.6(5)	1.0(9)	4.6*	1(2)	−5(3)
	S_0^2	0.62(6)			0.6(1)	

R, interatomic distance; σ^2, Debye–Waller factor along bond direction; E_0, phase shift correction; S_0^2, amplitude reduction factor (fixed values are marked with *).

comprises mixture of ionic, covalent and metallic bond. A simple estimate on the basis of bond valence sums implies that all the bonds in PbTe:Yb (metal–tellurium, metal–metal and tellurium–tellurium) are more ionic than in pure PbTe. Taking the ionic radii $R_i(Yb^{2+}) = 1.16$ Å, $R_i(Yb^{3+}) = 1.008$ Å, $R_i(Pb^{2+}) = 1.20$ Å, $R_i(Te^{2-}) = 2.21$ Å [19], one derives the following bond lengths: R(Pb–Te) = 3.41 Å, R(Yb^{2+}–Te) = 3.37 Å, R(Yb^{3+}–Te) = 3.218 Å. Our experimentally observed Yb–Te distance can be obtained by appropriate mixture of Yb^{2+}–Te and Yb^{3+}–Te bonds estimated this way. The increased iconicity is in accordance with observed increase of the PbTe:Yb bang gap with Yb concentration [9].

To reveal how the PbTe lattice accommodates these variations of Yb valence, Debye–Waller (DW) factors (σ^2) were analyzed. DW factors contain contribution both from configurational and thermal disorder of the distances and give direct information about structural disorder in the investigated system. Low temperature measurements allow to extract the information about configurational disorder, since the thermal vibrations are largely suppressed. The low temperature DW factor σ^2_{Pb-Te} is twice as high as σ^2_{Yb-Te}, which is inside experimental uncertainties the same as σ^2_{Te-Pb}. The similar relation exists between the second coordination atoms' DW

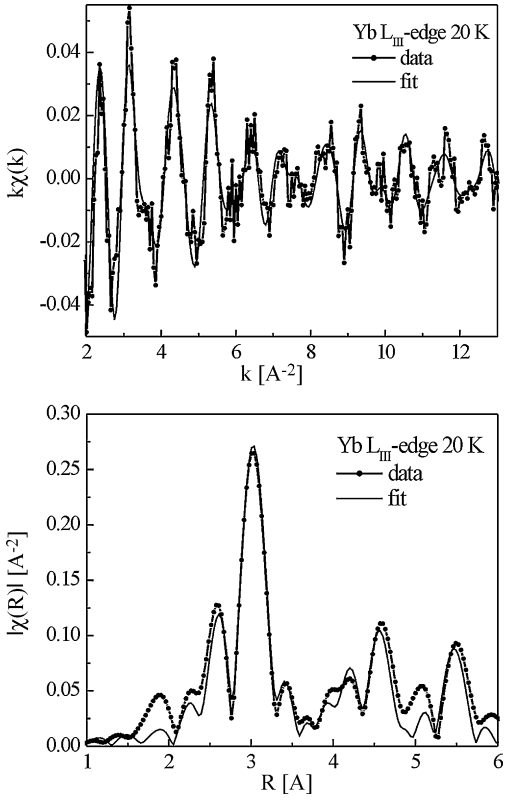

Fig. 3. Fits in k- and R-space of PbTe:Yb(1.3 at.%) EXAFS spectra taken at Yb L_{III}-edge at 20 K.

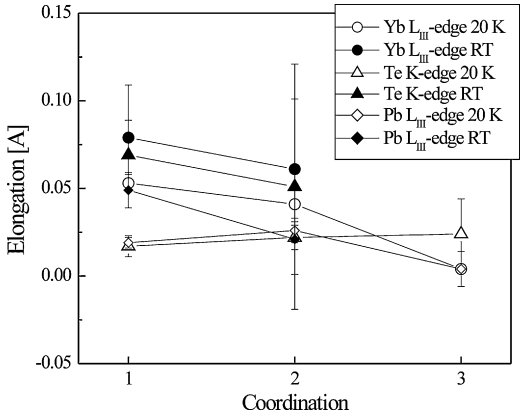

Fig. 4. Elongations of PbTe:Yb(1.3 at.%) distances in reference to pure PbTe.

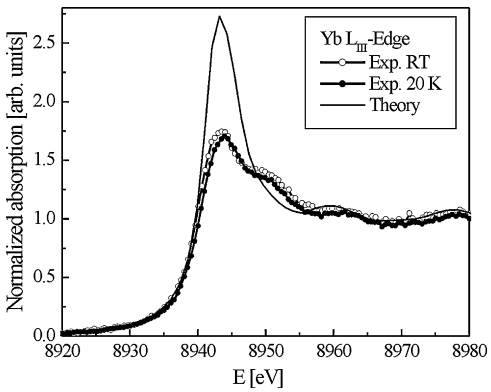

Fig. 5. The experimental XANES spectra of PbTe:Yb(1.3 at.%) taken at Yb L_{III}-edge (at 20 K and RT), and the model XANES spectrum of Yb placed at regular PbTe lattice position.

factors, $\sigma^2_{Pb-Pb} \approx \sigma^2_{Te-Te}$ (see Table 1). The facts that the same Pb–Te bond has markedly different DW factor (as seen from two different edges), and that Pb–Pb bonds have the largest DW factor, can in part be ascribed to the larger mean square displacement of Pb, $\langle u^2_{Pb}\rangle$, in comparison to that of Te, $\langle u^2_{Te}\rangle$ [20]. However, since the effect should not be that much pronounced on temperatures as low as 20 K, it means that Pb sub-lattice is to a quite extent affected by Yb presence. Tellurium sub-lattice, on the other side, at 20 K well accommodates Yb-induced stress, which is reflected through low DW factor. At RT, DW factors from all elemental edges and for both the first and the second coordination are approximately an order of magnitude larger than at 20 K, implying predominant influence of thermal vibrations to structural disorder.

The amplitude reduction factor S^2_0, both estimated by the procedure described in Section 2 and determined in the fitting procedure (see Table 1), is approximately 20% smaller than theoretically predicted, although it increases in the right direction from lighter towards heavier elements. This result could be due to some experimental uncertainty (such as inappropriate detector dead time correction), but it could also indicate the presence of highly distorted regions in the investigated sample.

3.2. XANES

The experimental Yb L_{III}-edge XANES spectra taken at 20 K and RT, together with the model XANES spectrum of Yb placed at regular PbTe lattice position are presented in Fig. 5. The model spectrum white line is characterized by one intensive peak, whereas the experimental spectra (which look almost identical at the two temperatures) have their white line composed of two distinct peaks separated by approximately 7 eV. In both experimental and in model spectrum the main peak at the absorption edge is positioned at ≈8943.5 eV, and corresponds to Yb^{2+} configuration [21]. The second peak in the experimental spectra at ≈ 8950 eV corresponds to Yb^{3+} [21]. The presence of Yb^{3+} in the sample also explains the reduced intensity of the experimental white line. In the higher energy region the spectra completely match, indicating that the local structure of the first two coordination shells only are affected by Yb presence, in agreement with the EXAFS results.

To determine the fraction of divalent and trivalent Yb ions in the sample, the linear peak fit analyses was conducted, and the results are presented in Fig. 6. The normalized XANES spectrum was fitted with two arctangent functions representing the L_{III}-edge absorption and two Lorentzian functions representing the white line. From the relative intensities of the two Lorentzian functions it was determined that at 20 K approximately 88% of Yb atoms

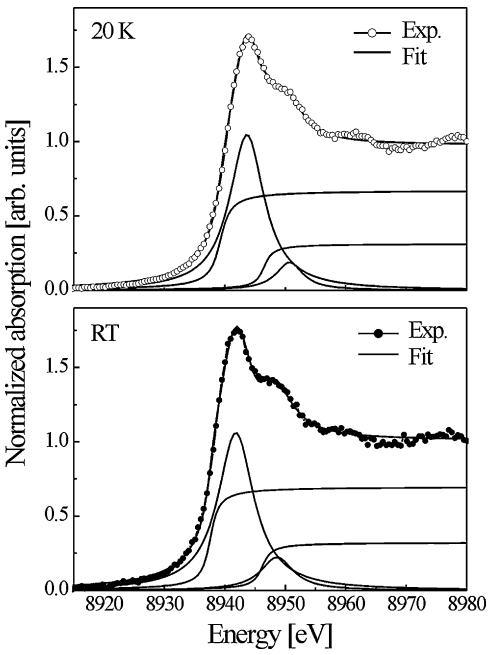

Fig. 6. Fit of PbTe:Yb(1.3 at.%) XANES spectrum taken at Yb L_{III}-edge at 20 K and at RT.

are in divalent state, and the remaining 12% are in trivalent state, leading to the mean valence of 2.12+. At RT, the amount of Yb^{3+} ions increases to 16%, and the mean valence to 2.16+. The Yb–Te distance evaluated by taking the upper ratio of Yb^{2+} and Yb^{3+} ions slightly exceeds that obtained from EXAFS spectra analysis, which implies that Yb–Te bonds in PbTe:Yb are not completely ionic.

Presence of Yb^{3+} cannot be explained as due to existence of a different impurity phase, since inside PbTe lattice Yb occupies the same crystallographic site as Pb which it replaces. Given that our EXAFS and XANES spectra analysis strongly support the NaCl-type structure of the investigated sample, it is then more likely that Yb is in intermediate valent ground state which comprises a mixture of $4f^{14}$ and $4f^{13}$ states. Induced by hybridization between localized 4*f* and conduction electrons, such a ground state is believed to be responsible for the valence instabilities phenomena observed in many rare-earth based compounds [22]. Another explanation could be the self-compensation effect, proposed in [7,8], which assumes the formation of native acceptors to compensate for the donor effect of doping. Detailed band structure calculations, necessary to resolve these doubts, are in progress.

4. Conclusion

The paper presents results of the X-ray Absorption Fine Structure (XAFS) measurements performed on uniformly doped PbTe:Yb (1.3 at.%) at 20 K and RT. From the analysis of the near edge (XANES) region of the absorption spectra the mixed-valence behaviour of Yb is revealed. It was found that at 20 K the mean valence of Yb is 2.12+, and that does not change significantly with temperature (2.16+ at RT). The high energy region of the absorption spectra (EXAFS) revealed that Yb incorporation causes deformation of the host PbTe lattice which is manifested through extension of the nearest-, and next-nearest neighbour distances around all atoms in the compound. The effect is more pronounced around Yb impurity, which altogether contradicts previously observed contraction of PbTe:Yb lattice for the same impurity concentration.

Acknowledgements

The authors gratefully acknowledge HASYLAB for providing the beamtime, and X1 beamline staff, in particular Dr. E. Welter and Dr. A. Webb, for their assistance during the XAFS measurements. This work was supported by Serbian Ministry of Science and Technological Development under the Grant 141009-Physics.

References

[1] S.N. Chesnokov, D.E. Dolzhenko, I.I. Ivanchik, D.R. Khokhlov, Infrared Phys. Technol. 35 (1994) 23–31.
[2] V. Osinniy, A. Jędrzejczak, W. Domukhovski, K. Dybko, B. Witkowska, T. Story, Acta Phys. Pol. A 108 (2005) 809–816.
[3] Z.H. Dughaish, Physica B 322 (2002) 205–223.
[4] K.F. Hsu, S. Loo, F. Guo, W. Chen, J.S. Dyck, C. Uher, T. Hogan, E.K. Polychroniadis, M.G. Kanatzidis, Science 303 (2004) 818–821.
[5] T.C. Harman, P.J. Taylor, M.P. Walsh, B.E. LaForge, Science 297 (2002) 2229–2232.
[6] E.P. Skipetrov, N.A. Chernova, E.I. Slyn'ko, Y.K. Vygranenko, Phys. Status Solidi (b) 210 (1998) 289–293.
[7] E.P. Skipetrov, N.A. Chernova, E.I. Slyn'ko, Y.K. Vygranenko, Phys. Rev B66 (2002) 085204(5).
[8] E. Skipetrov, E. Zvereva, L. Skipetrova, B. Kovalev, O. Volkova, A. Golubev, E. Slyńko, Phys. Status Solidi (b) 241 (2004) 1100–1105.
[9] S.K. Das, R. Suryanarayanan, J. Appl. Phys. 66 (1989) 4843–4845.
[10] B.A. Volkov, L.I. Rabova, D.R. Khokhlov, Phys. Usp. 45 (2002) 819–846.
[11] I. Radisavljević, N. Ivanović, N. Novaković, N. Romčević, H.-E. Mahnke, X-ray Spectrom. 36 (2007) 150–157.
[12] I. Radisavljević, N. Novaković, N. Ivanović, N. Romčević, M. Manasijević, H.-E. Mahnke, Physica B 404 (2009) 5032–5034.
[13] B. Ravel, M. Newville, J. Synchrotron Radiat. 12 (2005) 537–541.
[14] D.C. Koningsberger, R. Prins, X-ray Absorption-Principles, Applications, Techniques of EXAFS, SEXAFS and XANES, John Wiley & Sons, Chichester, 1987.
[15] A.L. Ankudinov, B. Ravel, J.J. Rehr, S.D. Conradson, Phys. Rev. B58 (1998) 7565–7576.
[16] Landolt-Börnstein, Group III condensed matter, Volume 41D, in: O. Madelung, U. Rössler, M. Schulz (Eds.), Non-Tetrahedrally Bonded Binary Compounds II, Springer-Verlag, 2000.
[17] CRC Handbook of Chemistry and Physics, 1st Student Edition, CRC Press, Boca Raton, FL, USA, 1988.
[18] A. Nicorici, V. Shklover, A.J. Todosiciuc, Optoelectron. Adv. Mat 10 (2008) 860–861.
[19] R.D. Shannon, Acta Cryst. A32 (1976) 751–767.
[20] C. Keffer, T.M. Hayes, A. Bienenstock, Phys. Rev. Lett. 21 (1968) 1676–1678.
[21] F. Grandjean, G.J. Long, B. Mahieu, J. Yang, G.P. Meisner, D.T. Morelli, J. Appl. Phys. 94 (2003) 6683–6691.
[22] D. Malterre, J. Durand, A. Siari, A. Menny, G. Krill, Marchal, J. Phys. Colloq. 49 (1988), C8-1361-C8-1362.